Limnol. Oceanogr., 59(6), 2014, 1839–1852
© 2014, by the Association for the Sciences of Limnology and Oceanography, Inc.
doi:10.4319/lo.2014.59.6.1839

The asymmetry of the underwater horizontal light field and its implications for mirror-based camouflage in silvery pelagic fish

Sönke Johnsen,[1,*] Ewa Gassmann,[2] Rick A. Reynolds,[2] Dariusz Stramski,[2] and Curtis Mobley[3]

[1] Biology Department, Duke University, Durham, North Carolina
[2] Marine Physical Laboratory, Scripps Institution of Oceanography, University of California–San Diego, La Jolla, California
[3] Sequoia Scientific, Bellevue, Washington

Abstract

Many pelagic species, particularly teleost fish, have silvered lateral surfaces that are thought to primarily serve as a form of camouflage. The underlying argument is that the underwater light field is cylindrically symmetrical around the vertical axis; thus a vertical mirror reflects a region of the water column that matches the region directly behind the mirror. However, the degree of symmetry of the underwater light field itself has not been assessed. Modeled underwater radiances from the surface to a depth of 100 m using measured profiles of inherent optical properties and HydroLight radiative transfer software showed that the horizontal light field under sunny conditions was asymmetrical over a wide range of solar elevations. In addition, the maximum asymmetry at 100 m occurred not when the sun was near the horizon, but when it was 45° above it. We validated these modeled results in Hawaiian waters using a modification of a commercial radiometer. Both modeled and measured radiances showed that the inherent contrast of silvery fish was typically higher at longer wavelengths. However, models of the sighting distances of these surfaces showed that sighting distance was greatest at the peak wavelength of the downwelling irradiance (~480 nm). The modeled and measured asymmetry of the horizontal light field implies that mirror camouflage is not always as successful as originally thought and suggests that there may be further refinements for this form of crypsis that have not been previously considered.

In the pelagic realm, there is no place to hide except in plain sight. Thus, camouflage is considerably more demanding than in other habitats, and three mechanisms have evolved—transparency, counterillumination, and mirrors—that are rare or nonexistent in other habitats (reviewed by McFall-Ngai 1990; Herring 2002; Johnsen 2014). Of these three strategies, mirrors are perhaps the most counterintuitive, and many who look at the silvered sides of herrings, sardines, and other teleosts are surprised to learn that they function as camouflage. The structure and optics of silvery fish were first investigated in detail by Eric Denton (reviewed by Denton 1970, 1971; Herring 1994), who noted that a vertical and perfectly reflecting mirror in an underwater light field that is symmetrical about the vertical axis will always reflect light from a portion of the light field that has a radiance that matches the radiance that would be seen if one could look directly through the mirror (Fig. 1A). He then showed that even fish with curved sides orient their guanine-based structural reflectors within their scales so that they remain vertical, strongly suggesting that they have evolved to function as camouflage (Fig. 1B). In addition, he also found that—in certain fish—reflectors with less than 100% reflectance were tilted slightly upwards, so as to compensate by reflecting light from a higher and thus brighter portion of the light field. More recently, McKenzie et al. (1995), Levi-Lior et al. (2010), and Jordan et al. (2012) further investigated the underlying physics of the reflecting platelets themselves and found that they are optimized for high reflectance.

Together, these studies leave no doubt that at least one function of the mirrored sides of silvery pelagic fish is camouflage. However, to date, the success of this form of crypsis has not been quantified (though *see* Johnsen and Sosik 2003). Although the reflectors themselves have been studied in great detail and fit the requirements for camouflage, the other requirement—the cylindrical symmetry of the underwater light field—has been less studied. While it has been known for decades that the underwater light field eventually becomes symmetrical about the vertical axis at great depths regardless of solar elevation (reviewed by Jerlov 1976; Mobley 1994), and while radiance measurements at shallower depths have been made (Voss 1989; Wei et al. 2012), the specific question of the asymmetry of underwater radiance as a function of solar position and the way in which this asymmetry affects the crypsis of silvery fish has not been addressed.

This study takes a first step in investigating this issue by both modeling and measuring horizontal radiance in both the solar and antisolar azimuth (i.e., with a sensor pointing directly towards and directly away from the direction but not the elevation of the sun) as a function of solar elevation to a depth of 100 m in clear, oceanic water (Jerlov type I; Jerlov 1976) at six wavelengths (410, 440, 480, 520, 550, and 600 nm). These radiance values are then used to calculate the visual contrast of a silvery fish against the background water when the lateral side faces both towards and directly away from the solar azimuth and is 100% reflective. These contrast measurements are in turn combined with models and measurements of minimum contrast thresholds and water clarity to estimate horizontal sighting distances. In addition to this analysis of what are essentially the worst cases (i.e., the ones with the highest contrast), we calculated

* Corresponding author: sjohnsen@duke.edu

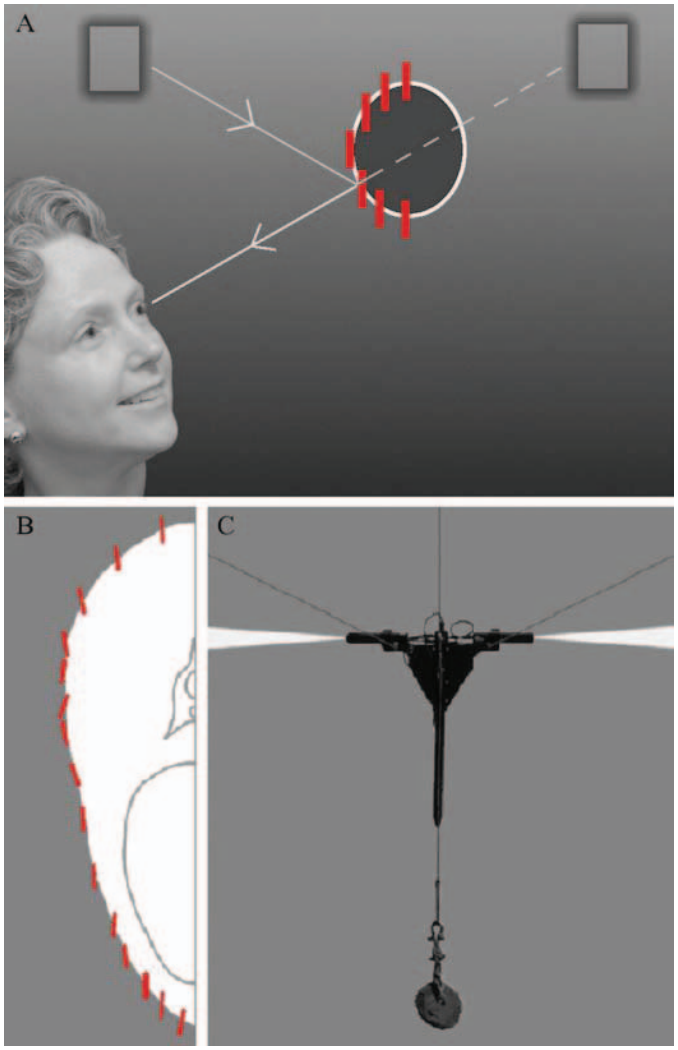

Fig. 1. (A) Light reflected from vertical mirrors underwater. The reflected radiance matches the radiance directly behind the animal if the underwater light field is symmetrical about the vertical axis. (B) Partial cross section of the bleak (*Alburnus alburnus*), showing the orientations of the reflecting plates within the scales. Modeled after Denton (1970). (C) Schematic diagram of the radiometer used to measure underwater horizontal radiance. The white regions show the fields of view of the two radiometers. The object hanging below the instrument is a weight to help the instrument maintain a vertical orientation. The two diagonal lines above the instrument represent the lines used to help ensure that the instrument maintained a constant azimuth.

contrast and sighting distances for all horizontal viewing conditions for the dominant wavelength at the solar elevation where horizontal radiance asymmetry is high (480 nm, with the sun 27.5° above the horizon). The results are discussed from the perspectives of both the silvery fish and the viewer to determine what the former can do to increase camouflage and what the latter can do to break it.

Methods

Contrast and sighting distance—In this study, we consider a 100% specularly reflective vertical mirror (i.e., the reflecting surface faces horizontally) that is oriented such that its reflecting surface either faces the azimuth of the sun or faces directly opposite it. This mirror is then viewed horizontally by an animal that is at the same depth and either between the mirror and the sun, or—in the second case—the mirror is between the viewer and the sun. In the first viewing condition, the mirror will always appear at least slightly brighter than the background water unless the sun is directly overhead (thus creating a symmetrical light field around the vertical axis). This is because the reflected radiance is the horizontal radiance in the solar azimuth (i.e., photons come from the azimuth of the sun: referred to hereafter as $L_0[\lambda]$, where λ is the wavelength of light in a vacuum), which is brighter than the background radiance, which in turn is in the antisolar azimuth (i.e., photons come from the azimuth 180° away from that of the sun: referred to hereafter as $L_{180}[\lambda]$). The Weber contrast (C) of this mirror viewed in this situation is then given by:

$$C(\lambda) = \frac{L_0(\lambda)}{L_{180}(\lambda)} - 1 \tag{1a}$$

In the second viewing condition, the mirror will always appear at least slightly darker than the background water (again, unless the sun is directly overhead), and its contrast is given by:

$$C(\lambda) = \frac{L_{180}(\lambda)}{L_0(\lambda)} - 1 \tag{1b}$$

In both viewing conditions, the mirror can be seen from a maximum distance (d) of:

$$d = \frac{1}{c(\lambda)} \ln\left(\frac{|C(\lambda)|}{C_{\min}(\lambda)}\right) \tag{2}$$

where $c(\lambda)$ is the beam attenuation coefficient of the water, and $C_{\min}(\lambda)$ is the minimum contrast threshold of the viewer (Duntley 1952, 1963; Mertens 1970). Thus, to determine the distance from which the mirror (or silvery fish) can be seen in these two viewing conditions, we need to know $c(\lambda)$, $C_{\min}(\lambda)$, and the ratio of $L_0(\lambda)$ and $L_{180}(\lambda)$. The first term is measured or computed from bio-optical models for clear, open-ocean waters (reviewed by Jerlov 1976; Mobley 1994), and we use the Rose-DeVries model for the second term (*see* below). Thus, the primary focus of this study is to determine the ratio of $L_0(\lambda)$ to $L_{180}(\lambda)$ (or its inverse for the second viewing condition) as a function of wavelength, depth, and solar elevation.

Radiative transfer model of horizontal radiance in the solar and antisolar azimuths—The horizontal radiances in the solar and antisolar azimuth ($L_0[\lambda]$ and $L_{180}[\lambda]$) were modeled using measured profiles of inherent optical properties and standard radiative transfer software (HydroLight 5.1, Sequoia Scientific). The ability of radiative transfer theory to accurately model oceanic radiance distributions has been validated by in situ measurements of selected radiances and irradiances in multiple studies (Mobley et al. 1993; Stramska et al. 2000). The agreement between modeled and measured radiances is particularly

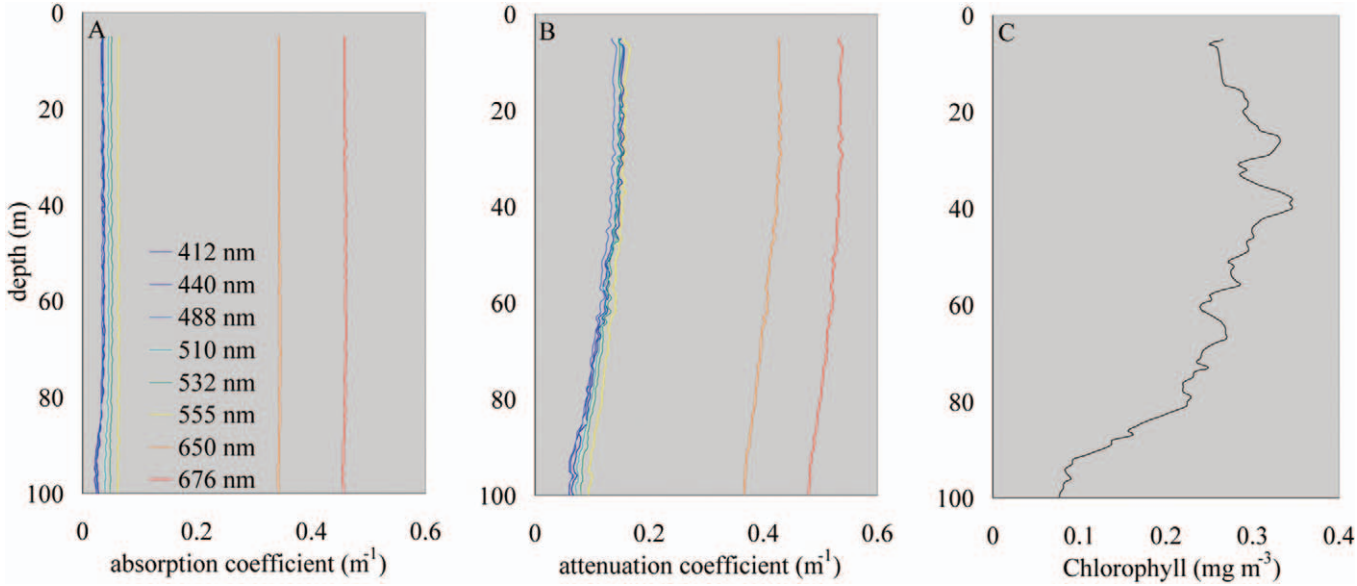

Fig. 2. The depth profiles of the inherent optical properties and chlorophyll *a* concentration that were input into HydroLight to calculate the underwater radiances. (A) Absorption coefficient. (B) Beam attenuation coefficient. (C) Chlorophyll *a* concentration.

good in tropical open oceanic waters, which are easily characterized (reviewed by Mobley 1994). In this study, the software was modified to increase the resolution of the elevation angle grid to allow for more precise placement of the sun.

Depth profiles of inherent optical properties and chlorophyll *a* (Chl *a*) concentration from tropical oceanic water (approximately Jerlov oceanic type I; Jerlov 1976) needed for the radiative transfer software were obtained from Drs. Andrew Barnard, Scott Pegau, and Ronald Zaneveld (College of Oceanic and Atmospheric Sciences, Oregon State University, Corvallis, Oregon), who collected them using a dual path, multiband absorption and attenuation meter (ac-9, Wetlabs) and fluorometer in the equatorial Pacific (10:05 h local time, 30 April 1996; 0°0′N, 177°21′W). Absorption and beam attenuation coefficients (at 412, 440, 488, 510, 532, 555, 650, and 676 nm) and Chl *a* concentration were measured at 1 m intervals to a depth of 138 m (Fig. 2). Absorption and attenuation measurements cannot be taken at any ultraviolet (UV) wavelengths with this instrument, which precludes the possibility of modeling the UV radiance distribution without making additional assumptions about the water absorption and scattering properties. This is unfortunate, considering the prevalence of UV vision in near-surface species (reviewed by Losey et al. 1999).

Underwater radiance distributions were calculated from 400 to 700 nm at 10 nm intervals and the surface to 100 m depth at 10 m intervals for the following solar elevations: 2.5°, 12.5°, 27.5°, 42.5°, 57.5°, 72.5°, 79.5°, 84.5°, 85.5°, 86.5°, 87.5°, and 88.5° (0° is sunrise or sunset). For each set of calculations, the sky was assumed to be cloudless, and the sea was assumed to be calm. The sky irradiance was calculated using the Radtran model (Gregg and Carder 1990), and the sky radiance angular distribution was calculated using the semi-empirical model given in Harrison and Coombes (1988). Both models account for atmospheric effects, such as the reddening of the sun as it approaches the horizon, and are well established. Pure water absorption was taken from Pope and Fry (1997), and the particle scattering phase function was an average-particle phase function based on measurements by Petzold (1977); tabulated values are given in Mobley (1994, table 3.10). Chlorophyll fluorescence was calculated from the measured Chl *a* concentration using a modeled phytoplankton absorption spectrum taken from Prieur and Sathyendranath (1981) and a fluorescence efficiency of 0.02 that was independent of excitation wavelength. Raman scattering by the water molecules was also included (Gordon 1999).

In situ measurements of horizontal radiance in the solar and antisolar azimuths—Depth profiles of hyperspectral horizontal radiance in both the solar and antisolar azimuths were taken at five solar elevations on a cruise of the R/V *Kilo Moana* off the coast of the Big Island of Hawaii in the tropical Pacific Ocean (28 May 2012 to 10 June 2012: *see* Table 1 for dates, times, and other parameters of measurements). The instrument was an Optical Profiler II (Hyperpro: Satlantic) fitted with two oppositely oriented HyperOCR hyperspectral radiance sensors (Satlantic; Fig. 1C). Each radiometer had an in-water full field of view of 8.5° (0.017 sr). The radiometric response of each sensor was calibrated by the manufacturer over the spectral range of 350 to 800 nm (i.e., UV-A to near-infrared). Measured spectra with 10 nm resolution were subsampled and recorded at a 3.3 nm wavelength interval. In addition to radiance, the profiler measured instrument tilt in two perpendicular axes (but unfortunately not azimuth), along with instrument depth and water temperature. Near the surface, data for $L_0(\lambda)$ were acquired

Table 1. Relevant parameters of the five casts of the horizontal radiometer. UTC, coordinated universal time.

Latitude	19°33.811′N	19°28.283′N	19°28.154′N	19°25.985′N	19°25.987′N
Longitude	156°18.885′W	156°21.316′W	156°21.465′W	156°20.003′W	156°20.017′W
Date (local)	03 June 2012	04 June 2012	04 June 2012	05 June 2012	05 June 2012
Time (h; local: UTC-10)	12:15–12:31	13:49–14:05	8:50–9:04	7:55–8:08	6:29–6:46
Solar elevation	86.5°–86.6°	66.2°–69.9°	40.3°–43.5°	27.7°–30.7°	8.8°–12.3°
Wind speed (m s^{-1})	6.4	4.9	3.3	1.4	1.3
Sky conditions	Clear	Partly cloudy (sun visible)	Partly cloudy (sun visible)	Clear	Clear

at a maximal sampling rate of approximately 3 Hz. For surface measurements of $L_{180}(\lambda)$, and for both sensors deeper in the water column, lower radiance signals required increased integration time (up to 2 s), which reduced the sampling rate to values as low as 0.4 Hz.

Five casts of the instrument were performed at times chosen to provide a broad range of solar elevation angles, which were calculated using the Astronomical Applications site of the U.S. Naval Observatory (http://aa.usno.navy.mil/). For each cast, the ship (which has excellent station-keeping abilities) was first turned so that the sun was within a degree of being directly to starboard. The instrument was lowered from the stern by a winch from a central cable fed through a pulley on the ship's A-frame, while the azimuth of the instrument was held nearly constant and perpendicular to the long axis of the ship via tension on lines attached to each end, which were held by two of the coauthors stationed at the port and starboard sides of the ship, respectively (*see* Fig. 1C). Thus, one radiometer was facing the sun and measuring $L_0(\lambda)$, and the other radiometer was facing away from the sun and measuring $L_{180}(\lambda)$. The instrument, which entered the water about 5 m from the stern, was lowered at 0.25–0.30 m s^{-1} until the radiance values at the peak wavelengths (typically around 480 nm) became indistinguishable from the instrument background noise (at depths ranging from 120 to 150 m, depending on solar zenith angle) and then raised back to the surface. Data were only collected while the instrument was being lowered. The bottom depth was greater than 4000 m for all five casts.

Analysis of in situ measurements of horizontal radiance—Raw data files and calibration information for the Hyperpro were first read into an ancillary Satlantic software program (SatCON). Stored voltages were then converted to calibrated units and exported to ASCII files. All remaining processing was subsequently done in MATLAB (Mathworks). Dark-noise levels associated with each gain (taken in situ using a movable shutter) were subtracted from the data. The arrays of profiler data and dark-corrected data from both radiometers were then interpolated to a common time vector (that of the radiometer with the slower sampling rate) to merge depth, tilt, and other ancillary measurements with the radiance data. The radiances were then interpolated to a common wavelength vector, spanning the spectral range of 350–800 nm at 2 nm resolution (though only the data from 400 to 700 nm are presented here). After rejecting all values measured with an instrument vertical tilt greater than 3°, the data were binned and averaged over 2 m depth intervals. We found that 2 m bins provided an acceptable compromise between depth resolution and data quality. We excluded data from the uppermost 10 m due to potential artifacts caused by reflections or shadowing by the ship itself. We also excluded radiance data that were less than 20% above the dark-noise level (*see* Fig. 3 for processed data from a single cast).

Estimation of sighting distances from modeled contrasts—Sighting distances were calculated using Eq. 2. Because the contrasts, $C(\lambda)$, derived from modeled and measured radiances were quite similar, we only used those derived from the modeled radiances. The beam attenuation coefficients, $c(\lambda)$, were taken from the inherent optical property measurements described earlier. The minimum contrast thresholds, $C_{\min}(\lambda)$, were calculated using the Rose–DeVries law, which states that the threshold is inversely proportional to the square root of the number of photons absorbed by the visual system (Cronin et al. 2014). We set the value of the threshold in our brightest condition (480 nm at 10 m depth when the solar elevation is 88.5°) to 0.02, which is a typical value for fish under bright, saturating illumination (reviewed by Douglas and Hawryshyn 1990). The contrast thresholds at all other depths, wavelengths, and solar elevations were then given by:

$$C_{\min}(\lambda,z,\theta) = 0.02\sqrt{\frac{480}{\lambda}\frac{L_0(480,10,88.5)}{L_0(\lambda,z,\theta)}} \qquad (3)$$

where z is depth, and θ is solar elevation.

Results

Contrasts of silvery fish based on modeled radiances—The modeled contrasts of a 100% reflective silvered lateral surface that faces the azimuth of the sun were quite high over much of the day and down to depths of 100 m (Fig. 4A). Indeed, with the exception of 600 nm light at deeper depths (where the majority of photons are nearly isotropically created by Raman scattering), the modeled contrasts were well above the minimum contrast threshold of 0.02, in some cases even two orders of magnitude higher (for comparison, the absolute value of the contrast of a black fish is one). Three major patterns emerged. (1) As might be expected due to the increased scattering of light, the contrasts decreased with depth at all wavelengths and for all solar elevations. (2) Seemingly paradoxically, the

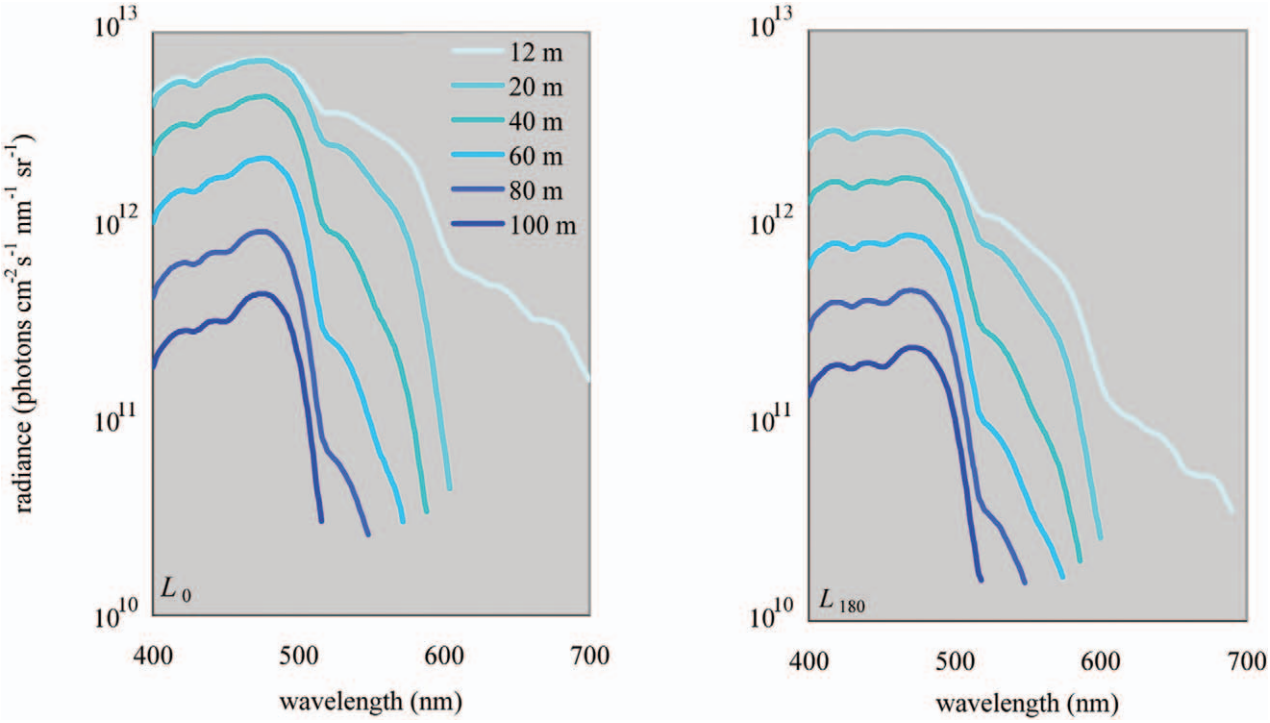

Fig. 3. Sample in situ horizontal radiances measured off the coast of the Big Island of Hawaii during the course of this study. In this case, the solar elevation ranged from 27.7° to 30.7° over the course of the cast. Note that the radiance in the solar azimuth (L_0) is typically greater than the radiance in the antisolar azimuth (L_{180}), and that this difference is more pronounced near the surface and at longer wavelengths.

contrasts were not highest at the lowest solar elevations. Instead, they were fairly low during sunrise and sunset, and then increased with solar elevation to a peak at an elevation between 30° and 45°. The exact location of the solar elevation that led to the highest contrast depended on depth, with the greatest contrast at 100 m being found at a solar elevation of 45°. The contrast then dropped as the sun rose higher, reaching zero as the sun approached the zenith. (3) The contrasts increased with increasing wavelength (up to 550 nm) at shallow depths but followed a more complex pattern at deeper depths (again due to the increasing proportion of Raman-scattered light at longer wavelengths and deeper depths).

The contrasts for the second viewing condition, where the fish is essentially silhouetted by sun, were considerably lower (Fig. 4C). In addition, the effects of solar elevation and wavelength on contrast were less pronounced.

Contrasts of silvery fish based on measured radiances—The contrasts of the mirror against the background water based on measured radiances followed the same trends displayed by those based on modeled radiances and matched the values fairly well given the significantly different methods involved (Fig. 4B). The contrasts generally decreased with depth and increased with wavelength at the shallower depths. Also, as was seen in contrasts based on modeled radiances, the peak contrast was not at the lowest solar elevation, but at an intermediate elevation. However, the limited number of solar elevations for which data were useable at greater depths made it uncertain whether the peak asymmetry still occurred at 45° solar elevation. Two significant departures of the modeled contrasts from the measured contrasts were that the latter typically had higher values at depth than the former, and the few measured contrasts that were available at 600 nm were substantially higher than those based on modeled radiances.

Sighting distances of silvery fish based on modeled radiances—Because oceanic water is highly transparent, particularly at blue wavelengths, the sighting distances calculated from the modeled radiances for both viewing conditions were quite high (Fig. 5). The sighting distances decreased uniformly with depth due to the increase in contrast threshold under dimmer illumination. However the sighting distances still reached 20–25 m near the surface for a broad range of wavelengths and again were maximal at solar elevations ranging from 30° to 45°. Finally, because sighting distance is a function of the logarithm of contrast (*see* Eq. 2), the substantially lower contrasts in the second viewing condition did not lead to as large drops in sighting distances as might be expected. Thus, fish that are silhouetted by the sun are visible at nearly the same distances as those that are lit by the sun.

Contrasts and sighting distances for all horizontal viewing and mirror azimuths at 480 nm with a solar elevation of 27.5°—Figure 6 shows the contrasts (both normalized and un-normalized) and sighting distances of a 100% reflective silvery fish as a function of both the azimuth of

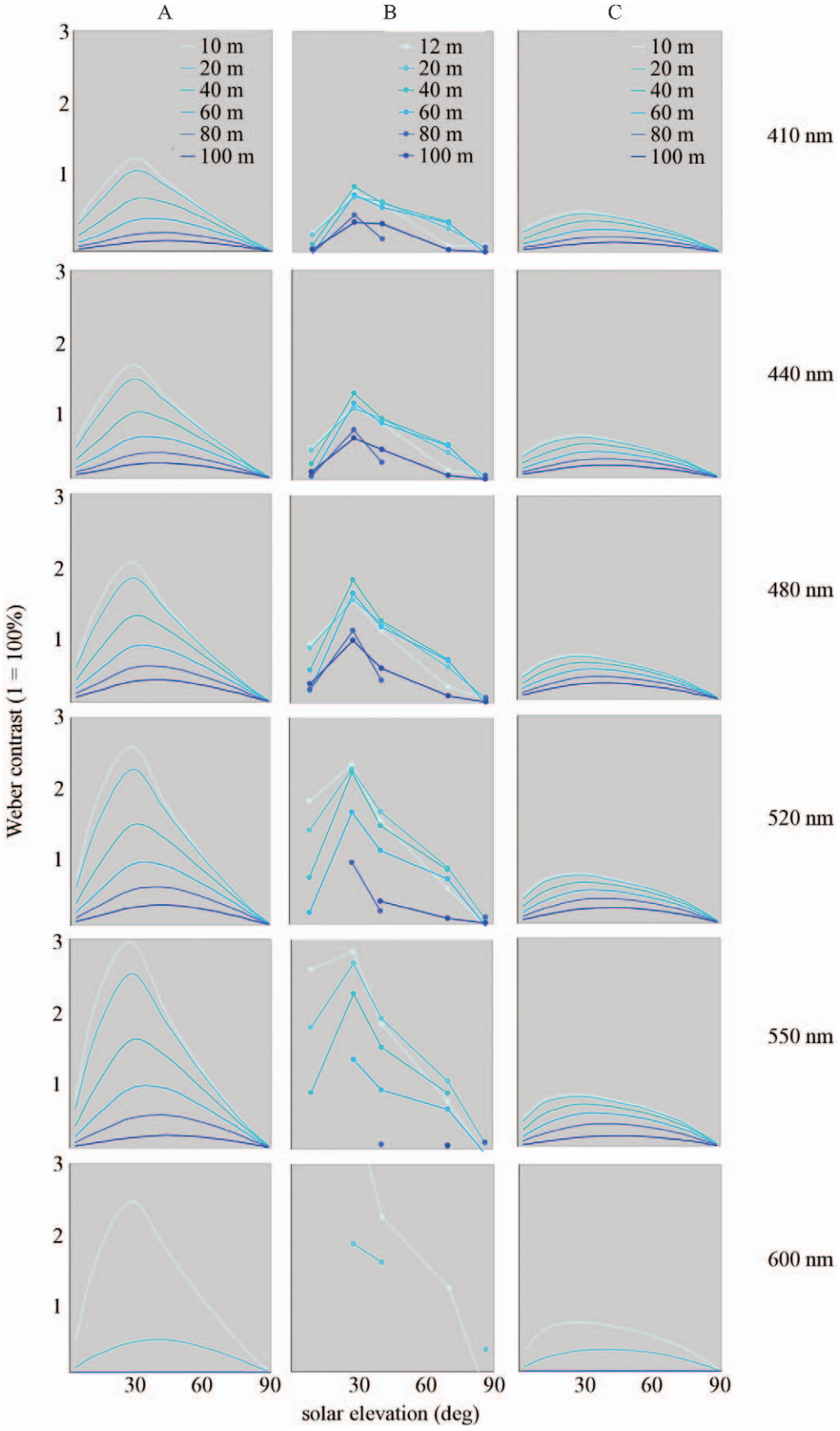
A
B
C
10 m
20 m
40 m
60 m
80 m
100 m
12 m
20 m
40 m
60 m
80 m
100 m
10 m
20 m
40 m
60 m
80 m
100 m
410 nm
440 nm
480 nm
520 nm
550 nm
600 nm
Weber contrast (1 = 100%)
3
2
1
30
60
90
solar elevation (deg)

the viewer and the direction the fish is facing. These data show that viewing geometries approximating the first condition had the highest contrasts and sighting distances, and geometries approximating the second condition had the second highest contrasts and sighting distances. Away from these two broad peaks, the contrasts and sighting distances decreased and reached zero for conditions where the background and reflected radiances were identical. The contrasts of the first viewing condition were much higher than those of the second condition at shallow depths, but this difference decreased with depth (Fig. 6B).

The contrasts averaged over all viewing and mirror azimuths were roughly one quarter of those in the first "worst case" viewing condition (Table 2). However, again, because sighting distances depend on the logarithm of the contrast, the average sighting distances at shallow depth were approximately half the sighting distances under the first viewing condition. At greater depths, the average sighting distances were far less than the peak sighting distance, primarily because the contrasts at depth were often below the relatively high minimum contrast thresholds of the viewer, resulting in a sighting distance of zero.

Discussion

The primary conclusion of this study is that a silvery fish can be roughly three to four times brighter than the background (as indicated by a Weber contrast of two to three) at surprisingly high solar elevations when viewed in certain directions at shallow depths. The exact sighting distances associated with these levels of contrast depend on the visual system of the viewer, but these can be high in clear waters. This of course assumes that the viewed fish is large enough to be seen at longer distances (*see* Aksnes and Utne [1997] for one model of sighting distance that incorporates apparent body size), but many hours of blue-water diving in the open ocean by the lead author confirm that large silvery fish (e.g., jacks, barracuda) can be seen at distances of tens of meters under the right viewing conditions.

However, this study examines the worst two cases, from the perspective of the camouflaging fish, where its nose faces an azimuth of either 90° or −90° and either its lit or silhouetted side is viewed full on. If the fish rotates away from this azimuth, or remains in the same orientation but is viewed from another azimuth, then the ratio of the reflected radiance to the background radiance decreases (*see* Fig. 6), until it reaches one when the long axis of the fish is parallel to the solar–antisolar axis. In other words, when a fish's anterior end directly faces towards or away from the sun, the radiance distribution is symmetrical about the long axis of the fish, and mirror camouflage is perfect regardless of the azimuth of the viewer, so long as the viewer and the fish are at the same depth. This strong effect of viewing azimuth and fish orientation is well known by anyone who has observed silvery fish underwater (or looked at clouds both towards and away from the sun), but this study shows that the contrasts are surprisingly large and occur at greater depths and higher solar elevations than is generally appreciated.

Effect of solar elevation—As any westbound evening commuter can attest, the asymmetry of azimuthal viewing in horizontal directions on land continues to increase as the sun sets, lessening only once the sun is so close to the horizon that it becomes dimmer and redder. However, this is not the case underwater. Instead, the asymmetry peaks at solar elevations between 30° and 45°, depending on depth. To our knowledge, this has not been previously reported, and the underlying reason has not been given an explicit mathematical treatment. Qualitatively however, it is due to the fact that underwater light is strongly scattered and absorbed compared to terrestrial light. Thus, the light field is more diffuse and depends more on the length of the path through the water. This second principle has been invoked to explain the fact that—at sufficiently large depths—the downward radiance (where photons travel vertically downwards) is always the greatest, regardless of the position of the sun, because the light from directly above has the shortest path through the water to the viewer and thus the least attenuation (reviewed by Mobley 1994). Returning to this study, at shallower depths (e.g., 60 to 100 m), it appears that once the sun is below an elevation of 30° to 45°, the relatively symmetrical blue sky and multiple scattering within the water play increasingly important roles in the underwater light field and make it more symmetrical. Indeed, if one divides the sky into a solar half (containing the sun) and an antisolar half (not containing the sun), the ratio of the irradiances of these two halves peaks when the sun is approximately 45° above the horizon, suggesting that—as depth increases—the horizontal radiance is affected by increasingly larger portions of the sky (*see* Fig. 7A). However, this is far from a formal explanation for the fact that asymmetry is maximal at this solar elevation at depths of 100 m, and further rigorous analysis is needed.

←

Fig. 4. (A) Contrast of a 100% reflective vertical mirror that faces the solar azimuth and is viewed horizontally from that direction (first viewing condition). The contrasts are based on radiances modeled using measured inherent optical properties and radiative transfer software. (B) Contrast of a 100% reflective vertical mirror that faces the solar azimuth and is viewed horizontally from that direction. The contrasts are based on measured radiances. (C) Absolute values of the contrast of a 100% reflective vertical mirror that faces opposite the solar azimuth and is viewed horizontally from that direction (second viewing condition). These contrasts are based on radiances modeled using measured inherent optical properties and radiative transfer software. Because the sun is behind the fish in this second viewing condition, the fish is darker than the background radiance.

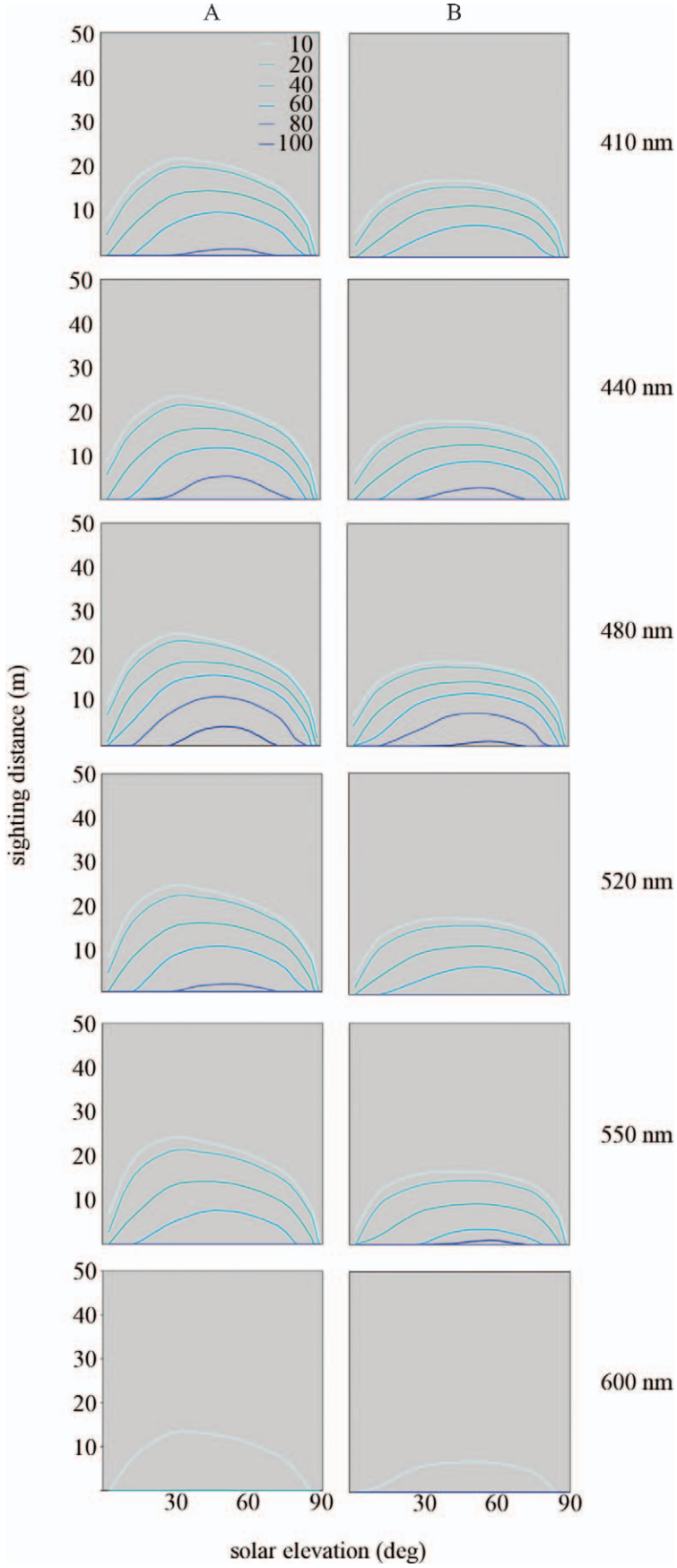
A
B
10
20
40
60
80
100
410 nm
440 nm
480 nm
520 nm
550 nm
600 nm
sighting distance (m)
solar elevation (deg)
50
40
30
20
10
30
60
90

Regardless of the exact optical mechanism, however, the fact that asymmetry peaks not at sunrise and sunset but during midmorning and midafternoon (and even midday for many nontropical latitudes over much of the year; *see* Fig. 7B) has important biological implications. Instead of silvery fish being vulnerable only when the sun is near the horizon, they can be vulnerable for much of the day. This is interesting in light of a number of studies that suggest that aquatic species are more vulnerable to predation during crepuscular periods (Hobson 1972; Helfman 1981; McFarland et al. 1999). This has generally been attributed to species differences in adaptation from photopic to scotopic levels of illumination, but there has also been the casual assumption (Johnsen and Sosik 2003) that sunrise and sunset are the periods with the greatest light asymmetry, which could break the camouflage of both silvery and colored fishes. The data presented here show that this cannot be the case, except possibly at depths shallower than we modeled and measured.

Also, because the sun reaches higher elevations in the tropics, there is the open question of whether silvery fish species are relatively more common in tropical waters than at higher latitudes, where lower solar elevations would lead to reduced crypsis. To our knowledge, no study of the latitudinal distribution of silvery fish has been performed, but a casual survey of the larger oceanic silvery fish (e.g., Carangidae, Megalopidae) finds that they are more commonly associated with tropical waters. However, this could also be due to the fact that tropical waters tend to be clearer, thus creating the need for additional camouflage strategies.

Effect of wavelength—This study shows that the asymmetry of the horizontal light field is typically greater at longer wavelengths. The primary reason for this is that scattering decreases and absorption increases with wavelength (reviewed by Mobley 1994), creating a light field that is less diffuse and thus more affected by the position of the sun. However, this is countered by the fact that—at the longest wavelengths and at the deepest depths—the light field is nearly entirely composed of Raman-scattered light, which is nearly isotropically created, leading to a highly symmetrical distribution around the vertical axis and more uniform angular distribution of light (Marshall and Smith 1990; Berwald et al. 1998; Li et al. 2014).

At more typical wavelengths for vision, though, this implies that silvery fish have a higher inherent contrast at longer wavelengths. However, as was discussed by Johnsen (2014), a higher inherent contrast does not necessarily mean that an object can be seen from further away, and indeed this study shows that sighting distance tends to be maximal at the peak wavelength of underwater illumination (480 nm). This is due to three factors. (1) The attenuation of light (and thus contrast) is typically higher at longer wavelengths. (2) The amount of light available for underwater vision decreases as wavelength increases, leading to poorer contrast sensitivity. (3) Because the sighting distance depends on the logarithm of inherent contrast (Duntley 1952; Mertens 1970), an increase in contrast has a smaller effect than might be expected. Considering all three factors, one has a situation where a fish at longer wavelengths has a slightly higher inherent contrast, but this contrast is both attenuated more rapidly and seen by a visual system that cannot discern small levels of contrast as well as can be done at shorter wavelengths. Thus, the sighting distance is less.

These considerations suggest that both predators and prey wishing to detect silvery fish should use visual pigments that are most sensitive to the peak wavelengths of underwater illumination, which is the case for many pelagic fish (reviewed by Cronin et al. 2014). The exception to this might be animals that are viewing silvery fish from short distances, perhaps schools of silvery fish that also use the reflections as intraspecific signals. In this case, visual pigments with absorption spectra that peak at longer wavelengths would increase the contrast of the image.

Limitations of measurements—While the good agreement between the contrasts based on the modeled radiances with those based on the measured radiances suggests that the fundamental conclusions of the study are sound, there are nevertheless limitations in the measured radiances. First and foremost, the radiometers did not have compasses, and so we do not have direct confirmation of their azimuthal orientation at depth. The lines used to control their azimuth would also be of decreasing utility at greater depths, even though the exceptional width of the ship (~27 m) allowed the ends of the two lines to be significantly separated. However, the instrument always came back out of the water in the same orientation as it entered and was only deployed in exceptionally calm seas. This combined with the accurate station-keeping abilities of the R/V *Kilo Moana* suggest that the radiometers maintained a relatively constant azimuthal orientation. Finally, because the orientation chosen maximizes the difference between the two measured radiances (because one instrument faces the sun, and the other faces away from it), the contrasts based on the measured radiances are a lower estimate of the true contrast of the worst-case scenario.

Another limitation is that only five solar elevations were investigated. This was due to the difficulty of meeting the correct sky (clear) and sea (calm) states. However, these five casts do show a pattern that mimics that found in the models. Finally, the sensitivity of the radiometers limited us to the top 100 m in the blue portion of the spectrum and

←

Fig. 5. (A) Sighting distances of a 100% reflective vertical mirror that faces the solar azimuth and is viewed horizontally from that direction (first viewing condition). (B) Sighting distances of a 100% reflective vertical mirror that faces opposite the solar azimuth and is viewed horizontally from that direction (second viewing condition).

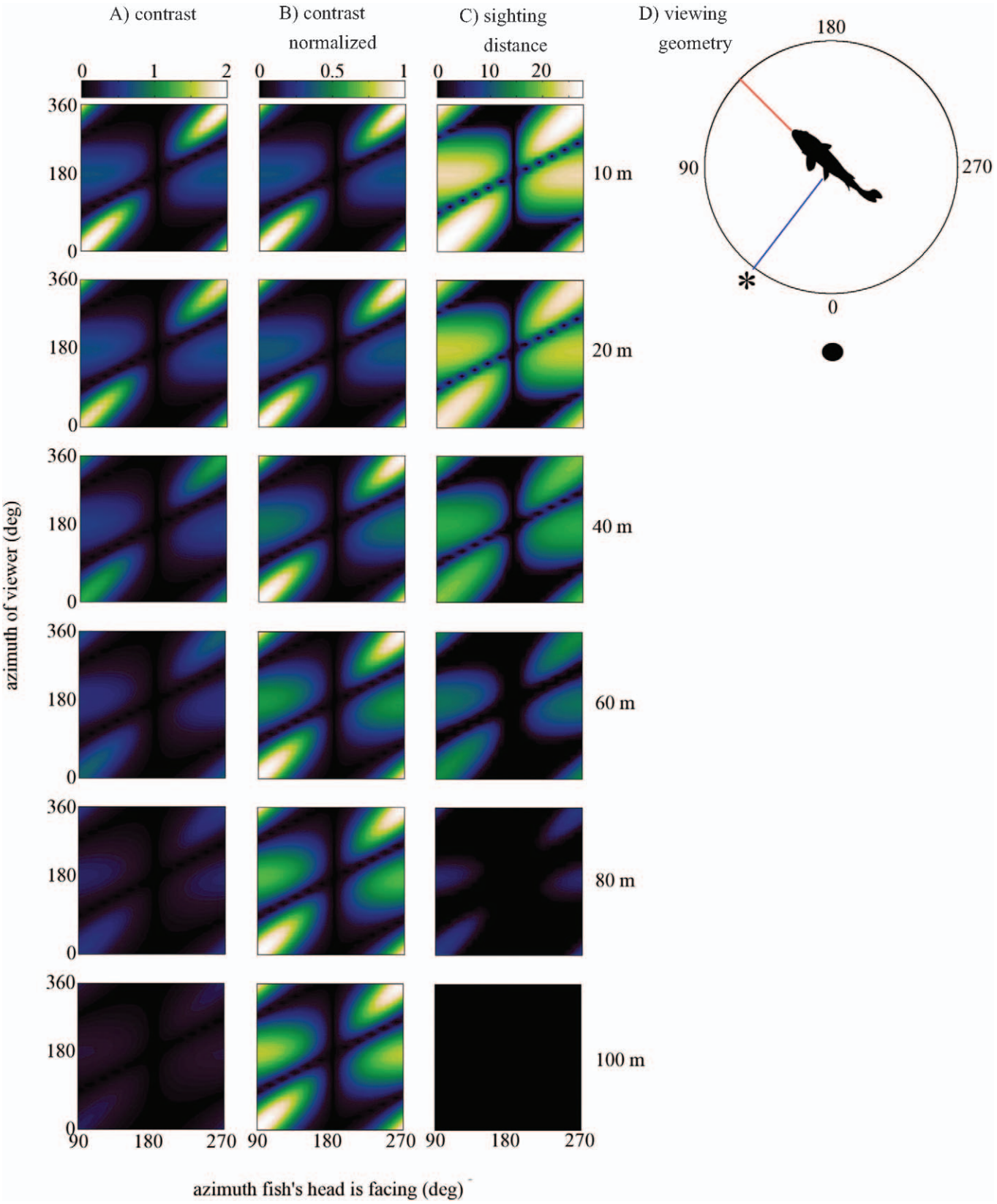

Fig. 6. (A) Contrasts of a 100% reflective silvery fish viewed horizontally as a function of the azimuth of the viewer and the azimuth the fish is facing. (B) Identical to the left column, but all graphs are normalized to a peak of one to better show detail. (C) Sighting distances of the fish based on the calculated contrasts. The wavelength is 480 nm and the solar elevation is 27.5° for all graphs. (D) The viewing geometry, with the black circle denoting the sun, the asterisk denoting the position of the viewer, and the red line denoting the direction the fish is facing. The data in all graphs are interpolated from the original 24 azimuths calculated by HydroLight.

Table 2. The maximal and average contrasts and sighting distances of a 100% reflective mirror viewed at a wavelength of 480 nm when the sun is 27.5° above the horizon. The maxima occur when the mirror faces the solar azimuth and is viewed horizontally from that direction. The averages are calculated over all possible azimuthal orientations of the mirror and azimuths of the viewer, with the fish and mirror constrained to be at the same depth. Note that while the average contrasts are typically one quarter of the maximum possible contrasts, the average sighting distances for depths up to 40 m are roughly half the maximum.

Depth (m)	Maximum contrast	Average contrast	Maximum sighting distance (m)	Average sighting distance (m)
10	2.01	0.47	27.8	15.1
20	1.79	0.43	25.6	13.6
40	1.24	0.33	19.8	9.3
60	0.80	0.24	14.5	5.1
80	0.49	0.16	7.3	1.1
100	0.30	0.10	0.0	0.0

considerably less at longer wavelengths. Future expeditions with more sensitive detectors should remedy these issues.

Implications for camouflaging organism—Given the asymmetry of the horizontal light field over much of the day, there are two primary solutions available to the camouflaging silvery fish. The first is to change its orientation. As mentioned above, a fish whose anterior end faces the solar or antisolar azimuth has approximately the same light field falling on each of its lateral surfaces (the match is not perfect due to the lensing effects of surface waves and the possible presence of clouds). Certain fish are known to use a sun compass for navigation (Hasler et al. 1958; Hasler and Schwassmann 1960; Goodyear and Ferguson 1969), but to our knowledge no one has investigated whether schools of pelagic fish tend to orient along a solar–antisolar axis. In coral reef and other benthic habitats, fish often school facing the current (reviewed by Leggett 1977), but in the open ocean, the fish are embedded in the current and no such orientation can exist, so the question of school orientation offshore and whether it is influenced by the azimuth of the sun is an open and important question.

Rather than change their azimuth, silvery fish in an asymmetric lighting environment could also tilt their bodies. If they tilt their dorsal surface toward the solar azimuth, the reflected radiance of the sunlit side will decrease, and the reflected radiance of the other side will increase, in both cases reducing contrast. However, the degree of tilt that optimally reduces contrast against a viewer at the same depth will not in general match the degree of tilt that is needed if the viewer is deeper or shallower than the fish, or at the same depth but viewing from another azimuth. Therefore, tilting is only successful for a limited set of cases.

In addition to tilting or rotating their bodies, fish could also alter the reflectance of their sides. While this study assumed that the reflectance of the silvery surfaces was always 100%, the value in actual fish is naturally at least somewhat lower (reviewed by Denton 1970). Thus, one solution is for fish to actively modulate the reflectance independently for each side, lowering it for the side facing the sun and raising it for the side facing away from the sun. While many fish appear to have a constant reflectance, others are known to be capable of changing their reflectance, either by altering the geometry of the reflectors themselves (Hiroshi et al. 1990) or by using pigments for which the expression or placement is under active control. The eyes could provide the visual feedback needed, as occurs in counterilluminating fish (reviewed by Johnsen 2014). While the surface facing away from the sun cannot have a reflectance greater than 100% and thus can never be perfectly camouflaged, in general a strategy of this sort would be useful. Currently, however, it is unknown whether any pelagic fish, silvered or otherwise, alters its reflectance to remain cryptic in a changing light field.

A simpler solution may be for the fish to have a reflectance that is either constant or changes with solar elevation, but is the same on both sides of the animal. While this may not result in perfect camouflage in all situations, it may nevertheless lower the sighting distance averaged over all fish orientations and viewer positions. While it is prohibitive to analyze this possibility over all viewer azimuths and depths (relative to the fish), it is possible to investigate the situation for which the fish and the viewer are at the same depth (i.e., the fish is viewed horizontally). In this case, the average sighting distance (d_{avg}, given in attenuation lengths) is:

$$d_{\mathrm{avg}} = \frac{1}{N^2}\sum_{i=1}^{N}\sum_{j=1}^{N}\ln\left(\frac{|C_{i,j}|}{C_{\mathrm{min}}}\right) \tag{4}$$

where N is the number of viewing azimuths (in this case 24), C_{min} is the minimum contrast threshold of the viewer, and $C_{i,j}$ is the absolute value of the contrast when the background light comes from azimuth j and the reflected radiance comes from azimuth i (the latter of which depends on both the azimuth of the viewer and the azimuthal orientation of the mirror). This last term is given by:

$$|C_{i,j}| = \left|\frac{RL_i}{L_j} - 1\right| \tag{5}$$

where R is the specular reflectance of the fish (which is assumed to be constant at all angles of incidence). The horizontal radiance distribution and the average sighting distance as a function of fish reflectance are shown in Fig. 8. In this limited case, the wavelength of the light is 480 nm, and the sun is 27.5° above the horizon. The minimum contrast threshold is again calculated using the

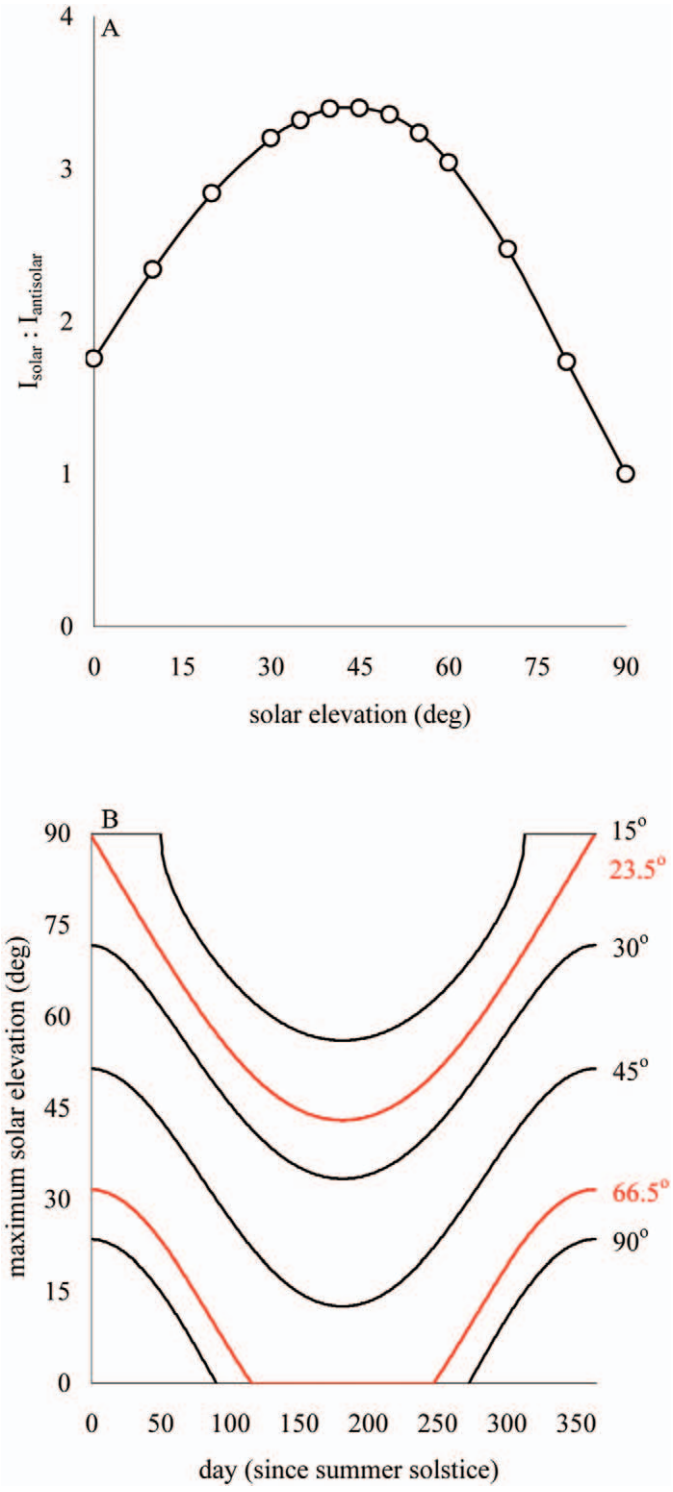

Fig. 7. (A) The ratio of the downwelling irradiance due to the half of the sky that contains the sun to the irradiance due to the half of the sky that does not contain the sun as a function of solar elevation. The boundary of the two halves of the sky is perpendicular to the solar–antisolar axis. The irradiances were calculated from a sky radiance model based on measurements taken using a radiometer that integrated spectral data from 0.3 to 3.0 μm (*see* Harrison and Coombes 1988). Therefore, no data for specific wavelengths are available. Note that the ratio peaks when the solar elevation is approximately 45°, providing a possible explanation for why underwater radiance symmetry at depth—where the light field is highly diffuse—also peaks when the sun is at 45°. (B) The greatest solar elevation over an entire day for a given latitude and day (relative to the summer solstice). The red line labeled 23.5° denotes the boundary of the tropics, and the red line labeled 66.5° denotes the Arctic and Antarctic Circles. Note that, for most latitudes and for much of the year, the solar elevation does not get above 45°.

Rose–DeVries law. The sighting distance, as mentioned above, is given in attenuation lengths rather than meters so that the curves depend only on the asymmetry of the light field and not on the fact that the water clarity changes with depth. It can be seen that the average sighting distance always decreases with increasing fish reflectance. In other words, a silvery fish is more cryptic on average than a black fish. However, the effect becomes stronger as the underwater light field become more symmetric. Thus, high reflectance is more useful at greater depths and at locations where the sun rises higher in the sky, and one would expect silvery fish to be more common at mesopelagic depths and in the tropics. As mentioned earlier, though, there are currently no data on the latitudinal or depth distribution of the reflectance of pelagic fish.

Implications for the viewing organism—For a viewer attempting to detect a pelagic organism using mirror camouflage, several strategies are possible. First, a circular search strategy is useful because under sunny conditions the horizontal light field is generally asymmetric for much of the day. A viewer circling a volume of water is more likely to detect a silvery fish within that volume, because at certain azimuths the reflected radiance will either be significantly higher or lower than the background radiance. This strategy works for other forms of pelagic camouflage as well (e.g., transparency, cryptic coloration) as any open-ocean diver searching for organisms can attest (Johnsen and Sosik 2003). Another strategy, which is not explored here, is for the viewer to continually change depth and thus viewing angle. This again may lead to a viewing position that maximizes contrast. Both strategies have been observed in pelagic predators, particularly in the presence of large schools of prey fish (Gallo Reynoso 1991; Similae 1997; McFarland et al. 1999), though, of course, they likely serve additional functions beyond visual detection, such as herding (Ikehara et al. 1978; Gallo Reynoso 1991; McFarland et al. 1999).

Acknowledgments

We thank Karin Akre, Laura Bagge, Christine Bedore, Nicholas Brandley, Eleanor Caves, Tom Cronin, Jamie Fergus, Yakir Gagnon, Daniel Speiser, Cynthia Tedore, Kate Thomas, and two anonymous reviewers for comments on the manuscript. We also thank Benjamin Wheeler, Scott Freeman, and the captain and crew of the R/V *Kilo Moana* for assistance with the in situ light measurements. S.J., E.G., D.S., and R.R. were supported in part by a grant from the Office of Naval Research (N00014-09-1-1053). C.D.M. was supported by HydroLight revenues.

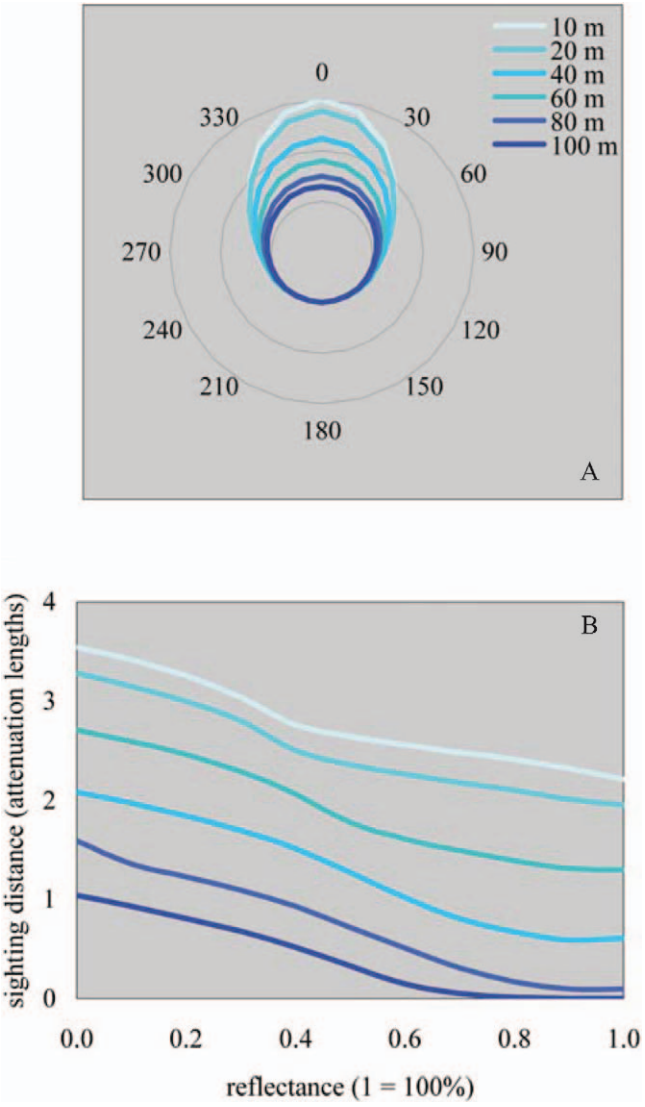

Fig. 8. (A) Polar plot of the underwater horizontal radiance (normalized by L_{180}) as a function of azimuth (the top of the plot being the solar azimuth). The wavelength of light is 480 nm, and the sun is 27.5° above the horizon. The gray circles are at unit intervals. (B) The average sighting distance of a silvery fish as a function of its specular reflectance. The fish is viewed horizontally, and the average is performed over all possible azimuth orientations of the fish and all possible azimuthal positions of the viewer. As in (A), the wavelength of light is 480 nm, and the sun is 27.5° above the horizon. The sighting distances are given in attenuation lengths. To convert to meters, one must divide by the beam attenuation coefficient. Note that, while average sighting distance always decreases with increasing reflectance, the effect is stronger when $L_0 : L_{180}$ approaches one, as happens either at greater depths or when the sun rises higher in the sky.

References

Aksnes, D. L., and A. C. W. Utne. 1997. A revised model of visual range in fish. Sarsia **82:** 137–147.

Berwald, J., D. Stramski, C. D. Mobley, and D. A. Kiefer. 1998. Effect of Raman scattering on the average cosine and diffuse attenuation coefficient of irradiance in the ocean. Limnol. Oceanogr. **43:** 564–576, doi:10.4319/lo.1998.43.4.0564

Cronin, T. W., S. Johnsen, N. J. Marshall, and E. J. Warrant. 2014. Visual ecology. Princeton Univ. Press.

Denton, E. J. 1970. On the organization of reflecting surfaces in some marine animals. Phil. Trans. Roy. Soc. Lond. B **258:** 285–313, doi:10.1098/rstb.1970.0037

———. 1971. Reflectors in fishes. Sci. Am. **224:** 65–72, doi:10.1038/scientificamerican0171-64

Douglas, R. H., and C. W. Hawryshyn. 1990. Behavioral studies of fish vision: An analysis of visual capabilities, p. 373–418. *In* R. H. Douglas and M. B. A. Djamgoz [eds.], The visual system of fish. Chapman and Hall.

Duntley, S. Q. 1952. The visibility of submerged objects. Final Report to Office of Naval Research.

———. 1963. Light in the sea. J. Opt. Soc. Am. **53:** 214–213, doi:10.1364/JOSA.53.000214

Gallo Reynoso, J. P. 1991. Group behavior of common dolphins (*Delphinus delphis*) during prey capture. Ana. Inst. Biol. Univ. Nacion. Auto. Mexico **62:** 253–262.

Goodyear, C. P., and D. E. Ferguson. 1969. Sun-compass orientation in the mosquitofish, *Gambusia affinis*. Anim. Behav. **17:** 636–640, doi:10.1016/S0003-3472(69)80005-9

Gordon, H. R. 1999. Contributions of Raman scattering to water-leaving radiance: A reexamination. Appl. Opt. **38:** 3166–3174, doi:10.1364/AO.38.003166

Gregg, W. W., and K. L. Carder. 1990. A simple spectral solar irradiance model for cloudless maritime atmospheres. Limnol. Oceanogr. **35:** 1657–1675, doi:10.4319/lo.1990.35.8.1657

Harrison, A. W., and C. A. Coombes. 1988. An opaque cloud cover model of sky short wavelength radiance. Sol. Energ. **41:** 387–392, doi:10.1016/0038-092X(88)90035-7

Hasler, A. D., R. M. Horrall, W. J. Wisby, and W. Braemer. 1958. Sun-orientation and homing in fishes. Limnol. Oceanogr. **3:** 353–361, doi:10.4319/lo.1958.3.4.0353

———, and H. O. Schwassmann. 1960. Sun orientation of fish at different latitudes. Cold Spring Harb. Symp. Quant. Biol. **25:** 429–441, doi:10.1101/SQB.1960.025.01.045

Helfman, G. S. 1981. Twilight activities and temporal structure in a freshwater fish community. Can. J. Fish. Aquat. Sci. **38:** 1405–1420, doi:10.1139/f81-187

Herring, P. J. 1994. Reflective systems in aquatic animals. Comp. Biochem. Physiol. **109A:** 513–546, doi:10.1016/0300-9629(94)90192-9

———. 2002. The biology of the deep ocean. Oxford Univ. Press.

Hiroshi, N., O. Noriko, and F. Ryozo. 1990. Light-reflecting properties of the iridophores of the neon tetra, *Paracheirodon innesi*. Comp. Biochem. Physiol. A **95:** 337–341, doi:10.1016/0300-9629(90)90229-L

Hobson, E. S. 1972. Activity of Hawaiian reef fishes during the evening and morning transitions between daylight and darkness. Fish. Bull. **70:** 715–740.

Ikehara, W., J. Atema, A. Brittain, J. Bardach, A. Dizon, and K. Holland. 1978. Reactions of yellowfin tuna to prey scents. Pac. Sci. **32:** 97.

Jerlov, N. G. 1976. Marine optics. Elsevier.

Johnsen, S. 2014. Hide and seek in the open sea: Pelagic camouflage and visual countermeasures. Ann. Rev. Mar. Sci. **6:** 369–392, doi:10.1146/annurev-marine-010213-135018

———, and H. M. Sosik. 2003. Cryptic coloration and mirrored sides as camouflage strategies in near-surface pelagic habitats: Implications for foraging and predator avoidance. Limnol. Oceanogr. **48:** 1277–1288, doi:10.4319/lo.2003.48.3.1277

Jordan, T. M., J. C. Partridge, and N. W. Roberts. 2012. Non-polarizing broadband multilayer reflectors in fish. Nature Photon. **6:** 759–763, doi:10.1038/nphoton.2012.260

Leggett, W. C. 1977. The ecology of fish migrations. Ann. Rev. Ecol. Sys. **8:** 285–308, doi:10.1146/annurev.es.08.110177.001441

Levy-Lior, A., and others. 2010. Guanine-based biogenic photonic-crystal arrays in fish and spiders. Adv. Funct. Mater. **20:** 320–329, doi:10.1002/adfm.200901437

Li, L., D. Stramski, D., and R. A. Reynolds. 2014. Characterization of the solar light field within the ocean mesopelagic zone based on radiative transfer simulations. Deep Sea Res. I: Oceanogr. Res. Pap., **87:** 53–69.

Losey, G. S., T. W. Cronin, T. H. Goldsmith, D. Hyde, N. J. Marshall, and W. N. McFarland. 1999. The UV visual world of fishes: A review. J. Fish. Biol. **54:** 921–943, doi:10.1111/j.1095-8649.1999.tb00848.x

Marshall, B. R., and R. C. Smith. 1990. Raman scattering and in-water optical properties. Appl. Opt. **29:** 71–84, doi:10.1364/AO.29.000071

McFall-Ngai, M. J. 1990. Crypsis in the pelagic environment. Amer. Zool. **30:** 175–188.

McFarland, W. N., C. Wahl, T. Suchanek, and F. McAlary. 1999. The behavior of animals around twilight with emphasis on coral reef communities, p. 583–628. *In* S. N. Archer, M. B. A. Djamgoz, E. R. Loew, J. C. Partridge, and S. Vallerga [eds.], Adaptive mechanisms in the ecology of vision. Kluwer.

McKenzie, D. R., Y. Yin, and W. D. McFall. 1995. Silvery fish skin as an example of a chaotic reflector. Proc. R. Soc. Lond. A **451:** 579–584, doi:10.1098/rspa.1995.0144

Mertens, L. E. 1970. In-water photography: Theory and practice. John Wiley & Sons.

Mobley, C. D. 1994. Light and water: Radiative transfer in natural waters. Academic Press.

———, and others. 1993. Comparison of numerical models for computing underwater light fields. Appl. Opt. **32:** 7484–7504, doi:10.1364/AO.32.007484

Petzold, T. J. 1977. Volume scattering functions for selected ocean waters, p. 150–174. *In* J. E. Tyler [ed.], Light in the sea. Dowden, Hutchinson, and Ross.

Pope, R. M., and E. S. Fry. 1997. Absorption spectrum 380–700 nm of pure water. II: Integrating cavity measurements. Appl. Opt. **36:** 8710–8723, doi:10.1364/AO.36.008710

Prieur, L., and S. Sathyendranath. 1981. An optical classification of coastal and oceanic waters based on the specific spectral absorption curves of phytoplankton pigments, dissolved organic matter, and other particulate materials. Limnol. Oceanogr. **26:** 671–689, doi:10.4319/lo.1981.26.4.0671

Similae, T. 1997. Sonar observations of killer whales (*Orcinus orca*) feeding on herring schools. Aquat. Mamm. **23:** 119–126.

Stramska, M., D. Stramski, B. G. Mitchell, and C. D. Mobley. 2000. Estimation of the absorption and backscattering coefficients from in-water radiometric measurements. Limnol. Oceanogr. **45:** 628–641, doi:10.4319/lo.2000.45.3.0628

Voss, K. J. 1989. Electro-optic camera system for measurement of the underwater radiance distribution. Opt. Eng. **28:** 241–247, doi:10.1117/12.7976940

Wei, J., R. van Dommelen, M. R. Lewis, S. McLean, and K. J. Voss. 2012. A new instrument for measuring the high dynamic range radiance distribution in near-surface sea water. Opt. Expr. **20:** 27024–27038, doi:10.1364/OE.20.027024

Associate editor: Thomas Kiørboe

Received: 19 February 2014
Amended: 07 July 2014
Accepted: 20 July 2014